Two-Dimensional Penning Ionization Electron Spectroscopy of Dichlorobenzenes: Orbital Reactivity and Anisotropic Interaction of Dichlorobenzenes with He*(2^3S)

Kohei Imura, Naoki Kishimoto, and Koichi Ohno*

Department of Chemistry, Graduate School of Science, Tohoku University, Aramaki, Aoba-ku, Sendai 980-8578, Japan

Received: May 22, 2001

Ionization of dichlorobenzenes with metastable He*(2^3S) atoms was studied by two-dimensional (collision-energy/electron-energy-resolved) Penning ionization electron spectroscopy. Collision energy dependence of the partial ionization cross sections (CEDPICS), which reflects the interaction potential energy between the molecule and He*(2^3S), showed anisotropic interaction around the molecules. The π and n (nonbonding) orbitals regions of the molecules showed attractive interactions. It was also found that the magnitude of attractive interaction around the Cl atom lone pair region perpendicular to the phenyl ring was *o*- > *p*- > *m*-$C_6H_4Cl_2$. Negative slopes of CEDPICS for σ type bands indicate an attractive effect for ionization reaction by a substitution of the Cl atom.

I. Introduction

Penning ionization[1] of several molecules with metastable rare gases, especially that of the metastable He* atom, has been widely investigated, since this reaction is one of the major processes for deexcitation of the metastable atoms. It has been recognized that the He* atom can be regarded as the simplest electrophilic reagent, because the He* atom extract an electron from a molecular orbital (MO) of the target molecule. Moreover, it has been suggested that anisotropy effects influence the Penning ionization probability. Therefore, it has been used to investigate not only the orbital reactivity but also the dynamics of particles on the anisotropic interaction potential energy surface.

Penning ionization process can be explained by the electron exchange model where an electron of the target MO is transferred into the inner vacant 1s orbital of the He*, which subsequently ejects the external electron in 2s orbital.[2] Then the mutual overlap of related orbitals for the electron exchange plays a central role. Experimental branching ratios of the Penning ionization can be roughly simulated by the exterior electron density (EED) of the target MOs exposed outside the molecular surface.[3,4] Thus, the Penning ionization electron kinetic energy spectrum (PIES) provides us information on the electron distribution of the target MOs exposed outside the boundary surface of collision.

It is obvious that the ionization cross section depends not only on the electron density distribution of the target MO but also on the characteristics of interactions between the colliding particles. Moreover, the collision energy (E_c) between the metastable atom and target molecule also plays a dominant role in the ionization event, since trajectories of the He* atom are expected to be influenced in some way, depending on the magnitude of interaction around the molecules with respect to the collision energy. Namely, the boundary surface of collision should depend both on the collision energy and also on the interaction of the colliding particles. If the ionization reaction is mostly governed by the attractive interaction, the ionization cross section should be enhanced at lower collision energies, because a slower He* atom can approach the reactive region effectively. On the contrary, if the ionization reaction is mostly governed by the repulsive interaction, the ionization cross section should be enhanced at higher collision energies, because a faster He* atom can approach the reactive region more effectively. Therefore, the observation of the collision-energy-dependent cross section provides valuable information about the interaction potential energy surface. Two-dimensional PIES (2D-PIES) has been recently developed in our laboratory,[5] in which ionization cross sections are determined as functions of both electron kinetic energy (E_e) and collision energy. This technique makes it possible to study the collision energy dependence of the partial ionization cross sections (CEDPICS) and collision-energy-resolved PIES (CERPIES), and thus the state-resolved measurement of partial cross sections for the various ionic state enables us to investigate anisotropic potential surface around the target molecule. 2D-PIES studies of several aromatic compounds (such as benzene,[6] polycyclic aromatic hydrocarbons,[7] heterocyclic compounds,[8] [2,2]-paracyclophane,[9] azines,[10] and substituted benzenes[11] (aniline, phenol, thiophenol), monohalogenobenzenes,[12] and difluorobenzenes[13]) with He*(2^3S) atoms have been reported so far.

Very recently, we have reported that the magnitude of attractive interaction around the F atoms with the metastable atom depends strongly on the substituent position for difluorobenzenes.[13] The magnitude of the attractive interaction around the $n_{||}$ and σ_{CF} orbital region was found to be *o*- > *m*- ∼ *p*-$C_6H_4F_2$. We have also reported that the interaction potentials of He*(2^3S) and C_2H_5X (X = Cl and F) molecules show a marked difference, especially around the halogen atom.[14] Anisotropic interactions of CH_3Cl and $CHCl_3$ with metastable rare gas atoms have been studied.[15−18] These results substantiate the importance of the interactions for Penning ionization. Therefore, the elucidation of the anisotropic interactions with the He* atom around Cl atoms and that of the substituent effect on the reactivity in dichlorobenzenes by using the characteristics of 2D-PIES measurements have considerable stereochemical significance because such elucidations provide further insight into the role of the electrophilic reactions.

10.1021/jp011970r CCC: $20.00
Published on Web 09/15/2001

II. Experimental Section

High purity samples, *o*-, *m*-, and *p*-$C_6H_4Cl_2$ were commercially purchased and purified by the several freeze−pump−thawed cycles. The experimental apparatus for He*(2^3S) Penning ionization electron spectroscopy and He I (584 nm, 21.22 eV) ultraviolet photoelectron spectroscopy has been reported previously.[6,19−21] Briefly, a metastable He*(2^1S,2^3S) beam was generated by a discharge, and the He*(2^1S) component was optically removed by a helium discharge lamp. Remaining byproducts, such as ionic and Rydberg species, are removed by an electric deflector. The Penning ionization of He*(2^3S) metastable atoms with the target molecules takes place at a reaction cell, and the kinetic energy of ejected electrons by the reaction was measured by a hemispherical electrostatic deflection type analyzer. We estimate the energy resolution of the electron energy analyzer to be 70 meV from the full width at the half-maximum (fwhm) of the $Ar^+(^2P_{3/2})$ peak in the He I ultraviolet photoelectron spectrum UPS. The observed PIES and UPS were calibrated by the transmission efficiency curve of the electron analyzer, which was alternatively determined by comparing our UPS data of several molecules with those by Gardner and Samson[22] and Kimura et al.[23] Calibration of the electron energy scale was made by reference to the lowest ionic state of N_2 mixed with the sample molecule in He I UPS (E_e = 5.639 eV)[24] and He* (2^3S) PIES (E_e = 4.292 eV).[25,26]

In the collision-energy-resolved experiments, 2D-PIES, the metastable atom beam was modulated by a pseudorandom chopper[27] rotating about 400 Hz and introduced into the reaction cell located about 500 mm downstream from the chopper disk with keeping constant sample pressure. The resolution of the electron analyzer was lowered to 250 meV in order to gain higher electron counting rates. Kinetic electron energies (E_e) were scanned by 35 meV steps. Similarly, the velocity distribution of the metastable He* beam was determined by measuring the intensity of secondary emitted electrons from the inserted stainless plate. The 2D Penning ionization data as functions of both E_e and t were converted by Hadamard transformation in which time dependent signals were cross-correlated with the complementary slit sequence of the pseudorandom chopper, and then the velocity dependence of the electron signals was obtained. The 2D Penning ionization cross section $\sigma(E_e,v_r)$ was obtained with normalization by the velocity distribution of He* $I_{He^*}(v_{He^*})$.

$$\sigma(E_e,v_r) = A[I_e(E_e,v_{He^*})/I_{He^*}(v_{He^*})](v_{He^*}/v_r)$$

$$v_r = [v_{He^*}^2 + 3kT/M]^{1/2}$$

where A, v_r, k, T, and M are proportionality constants, the relative velocity of metastable atoms averaged over the velocity of the sample molecule, the Boltzmann constants, the gas temperature (300 K), and the mass of the sample molecule, respectively. Finally, $\sigma(E_e,v_r)$ is converted to $\sigma(E_e,E_c)$ as functions of E_e and E_c by the following relation:

$$E_c = \mu v_r^2/2$$

where μ is the reduced mass of the reaction system.

III. Calculations

Interaction potential energies between a target molecule (M) and He*(2^3S) in various directions and angles were modeled by approximating the M-He*(2^3S) surfaces with those of Li-(2^2S)-M on the basis of the well-known resemblance between He*(2^3S) and Li(2^2S);[28] similar shapes for the velocity dependence of the total scattering cross section and for the location and depth of the attractive potential well for He*(2^3S) and Li(2^2S) with various atomic targets were obtained.[29−32] Recently, a precise estimate of the similarity[33] has been made for atomic targets; the well depths for the Li + Y (Y = H, Li, Na, K, Hg) systems were found to be 10% to 20% larger than those for He*(2^3S) + Y. Although for molecular targets M a direct comparison between the interactions of Li + M and He*(2^3S) + M has never been reported so far, the observed peak energy shifts between PIES and UPS, which were relevant to the interaction potentials between the reagents, were well-reproduced by the Li + M potentials calculations for numerous compounds.[21,34−39] Because of these findings and the difficulties associated with calculation for excited states, Li was used in this study in place of He*(2^3S). Thus, the interaction potential M-Li(2^2S), $V^*(R,\theta,\phi)$ (where R is the distance between Li atom and either Cl atom or the center of the benzene ring and θ and ϕ are angles defined in Figures 10b,c, 11b,c, and 12b,c), was calculated by moving the Li atom toward the halogen atom and keeping the molecular geometries fixed at the experimental values;[40,41] this assumption meant that the geometry change induced by the approach of a metastable atom was negligible in the collisional ionization process. For calculating the interaction potential, the standard 6-31+G* basis set was used, and the correlation energy correction was partially taken into account by using second-order Møller−Plesset perturbation theory (MP2).

We performed ab initio self-consistent field (SCF) calculations with 4-31G basis functions for *o*-, *m*-, *p*-$C_6H_4Cl_2$ in order to obtain electron density contour maps of MOs. In electron density maps, thick solid curves indicate the repulsive molecular surface approximated by van der Waals radii[42] (r_C = 1.7 Å, r_H = 1.2 Å, and r_{Cl} = 1.8 Å).

The ionization potentials were also calculated at the experimentally determined geometries using the outer valence Green's function (OVGF) method[43,44] for *o*-, *m*-, and *p*-$C_6H_4Cl_2$ with 6-311G** basis sets. All the calculations in this study were performed with the GAUSSIAN 98 quantum chemistry program.[45]

IV. Results

Figures 1−3 show the He I UPS and He*(2^3S) PIES of *o*-, *m*-, and *p*-$C_6H_4Cl_2$. The electron energy scales for PIES are shifted relative to those of UPS by the excitation energy difference between He I photons (21.22 eV) and He*(2^3S) (19.82 eV), namely, 1.40 eV. Band labels in UPS show orbital characters on the bases of their symmetries and bonding characters.

Collision-energy-resolved PIES (CERPIES) results obtained from the 2D spectra of *o*-, *m*-, and *p*-$C_6H_4Cl_2$ are shown in Figures 4−6. The CERPIES are shown for hot spectra at the higher collision energy (ca. 250 meV) and cold ones at the lower collision energy (ca. 100 meV). The relative intensities of the two spectra are normalized in the figures using the data of the log σ vs log E_c plots.

Figures 7−9 show the log σ vs log E_c plots of CEDPICS in a collision energy range of 90−300 meV for *o*-, *m*-, and *p*-$C_6H_4Cl_2$ with the calculated electron density maps. The CEDPICS was obtained from the 2D-PIES $\sigma(E_e,E_c)$ within an appropriate range of E_e (typical electron energy resolution of analyzer: 250 meV) to avoid the contribution from neighbor bands. The calculated electron density maps for s orbitals are shown on the molecular plane, and those for p orbitals are shown on a plane at a height of 1.7 Å (van der Waals radii of C atom) from

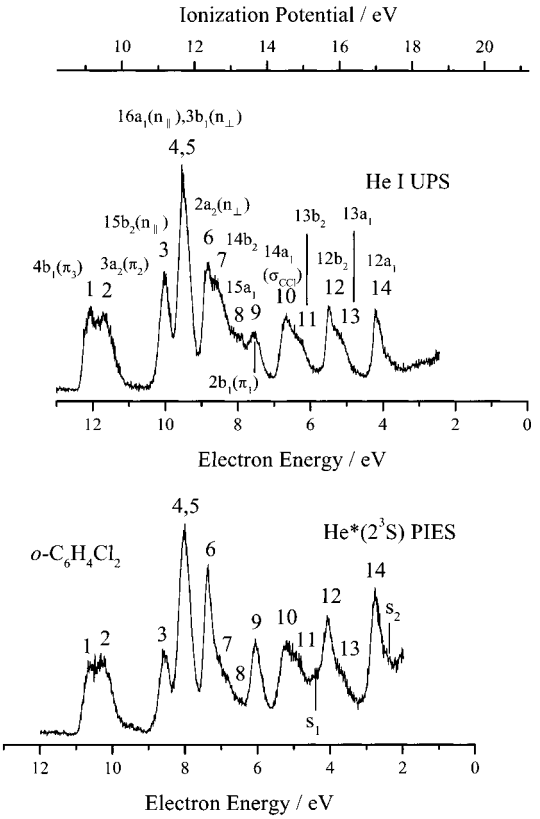

Figure 1. He I UPS and He*(2^{3}S) PIES spectrum of o-$C_6H_4Cl_2$. Average collision energy (60−400 meV) of PIES was ∼160 meV.

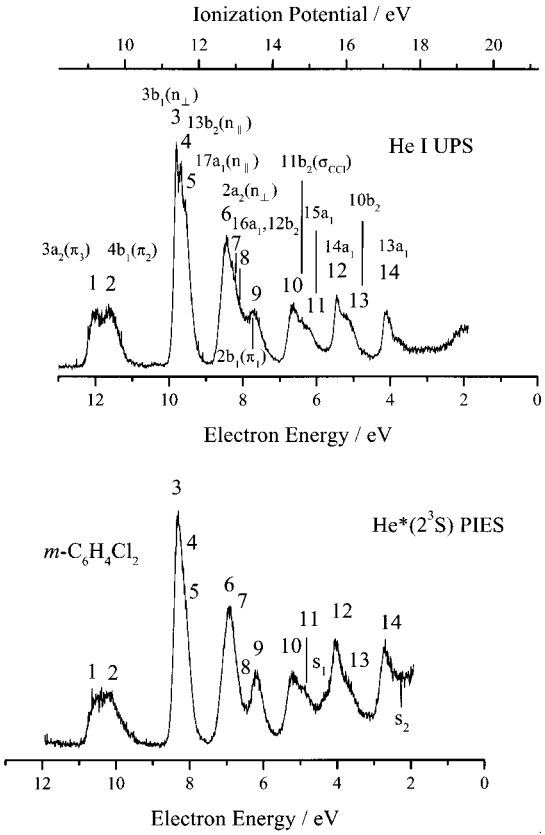

Figure 2. He I UPS and He*(2^{3}S) PIES spectrum of m-$C_6H_4Cl_2$. Average collision energy (60−400 meV) of PIES was ∼160 meV.

the molecular plane. At the right side of the figures, electron density maps for $\pi_{3,2,1}$ and $n_\perp$ orbitals were drawn on the plane defined in the figures.

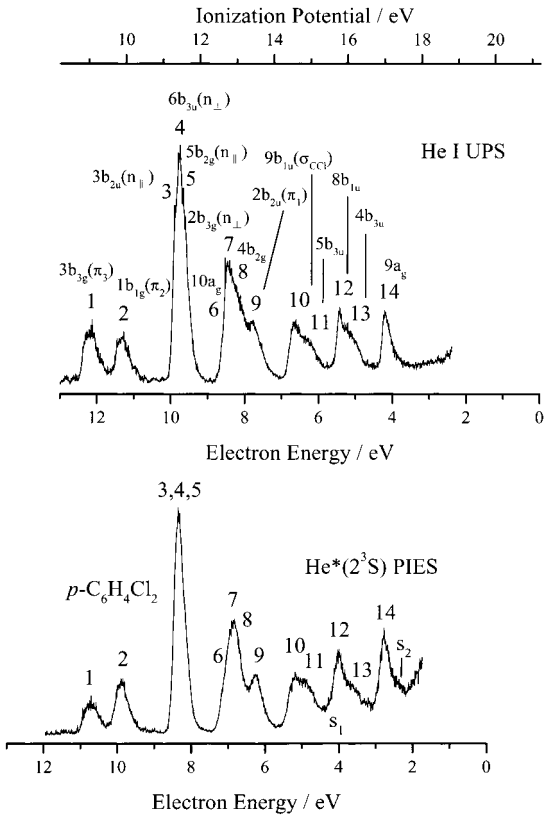

Figure 3. He I UPS and He*(2^{3}S) PIES spectrum of p-$C_6H_4Cl_2$. Average collision energy (60−400 meV) of PIES was ∼160 meV.

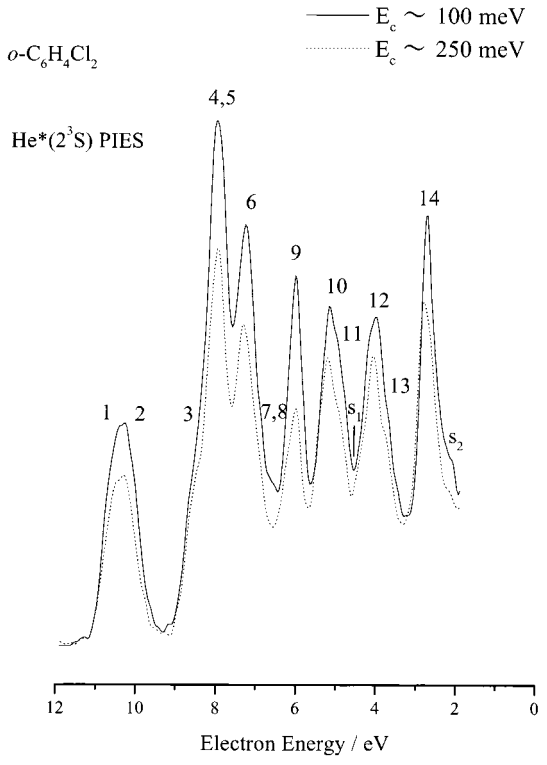

Figure 4. Collision-energy-resolved He*(2^{3}S) PIES of o-$C_6H_4Cl_2$. E_c denotes collision energy.

Tables 1−3 summarize experimentally observed and calculated ionization potentials (IPs), experimental peak energy shifts (ΔE), slope parameters of CEDPICS (m), and the assignment of the bands. Slope parameters are obtained from the log σ vs log E_c plots in a collision energy range for 90−300 meV by a

TABLE 1: Band Assignment, Ionization Potentials (IP/eV), Peak Energy Shifts (Δ*E*/meV), and Slope Parameters (*m*) for *o*-$C_6H_4Cl_2$

molecule	band	IP_{obsd}/eV	IP_{OVGF}/eV (pole strength)	orbital character	Δ*E*/meV	*m*
o-$C_6H_4Cl_2$	1	9.15	8.79(0.90)	$4b_1(\pi_3)$	-60 ± 70	−0.27
	2	9.50	9.37(0.90)	$3a_2(\pi_2)$	-10 ± 70	−0.31
	3	11.19	11.09(0.91)	$15b_2(n_{\|\|})$	-40 ± 60	−0.19
	4, 5	11.69	11.66(0.91)	$16a_1(n_{\|\|})$	-100 ± 60	−0.31
		11.69	11.68(0.88)	$3b_1(n_\perp)$	-100 ± 60	
	6	12.38	12.21(0.90)	$2a_2(n_\perp)$	-50 ± 60	−0.28
	7	12.65	12.93(0.90)	$14b_2$	-100 ± 100	−0.28
	8	13.2	12.97(0.90)	$15a_1$	-50 ± 120	
	9	13.60	13.89(0.83)	$2b_1(\pi_1)$	-150 ± 70	−0.44
	10	14.54	14.72(0.89)	$14a_1(\sigma_{CCl})$	-40 ± 70	−0.14
	11	14.85	14.87(0.88)	$13b_2$	0 ± 70	−0.21
	12	15.73	16.03(0.87)	$12b_2$	-10 ± 60	−0.18
	13	16.01	15.99(0.86)	$13a_1$	-100 ± 120	−0.16
	14	17.01	17.35(0.86)	$12a_1$	-20 ± 70	−0.13
	s_1	15.34[a]	–	–	–	−0.15
	s_2	17.44[a]	–	–	–	(−0.16)

[a] Obtained by He*(2^3S) PIES.

TABLE 2: Band Assignment, Ionization Potentials (IP/eV), Peak Energy Shifts (Δ*E*/meV), and Slope Parameters (*m*) for *m*-$C_6H_4Cl_2$

molecule	band	IP_{obsd}/eV	IP_{OVGF}/eV (pole strength)	orbital character	Δ*E*/meV	*m*
m-$C_6H_4Cl_2$	1	9.26	8.95(0.90)	$3a_2(\pi_3)$	-50 ± 70	−0.27
	2	9.58	9.41(0.90)	$4b_1(\pi_2)$	-30 ± 70	−0.31
	3	11.40	11.43(0.88)	$3b_1(n_\perp)$	-70 ± 60	−0.27
	4	11.52	11.36(0.91)	$13b_2(n_{\|\|})$	-100 ± 70	
	5	11.65	11.58(0.91)	$17a_1(n_{\|\|})$	-70 ± 70	
	6	12.77	12.81(0.90)	$2a_2(n_\perp)$	-100 ± 70	
	7, 8	12.9	12.99(0.90)	$16a_1$	–	−0.22
		13.0	13.04(0.90)	$12b_2$	–	
	9	13.49	13.79(0.83)	$2b_1(\pi_1)$	-130 ± 70	−0.28
	10	14.58	14.76(0.89)	$11b_2(\sigma_{CCl})$	0 ± 70	−0.11
	11	14.94	14.91(0.89)	$15a_1$	$+20 \pm 110$	−0.15
	12	15.76	16.03(0.87)	$14a_1$	-10 ± 80	−0.21
	13	16.04	16.02(0.86)	$10b_2$	-60 ± 120	−0.14
	14	17.11	17.48(0.85)	$13a_1$	$+30 \pm 70$	−0.05
	s_1	15.40[a]	–	–	–	−0.15
	s_2	17.53[a]	–	–	–	(−0.11)

[a] Obtained by He*(2^3S) PIES.

TABLE 3: Band Assignment, Ionization Potentials (IP/eV), Peak Energy Shifts (Δ*E*/meV), and Slope Parameters (*m*) for *p*-$C_6H_4Cl_2$

molecule	band	IP_{obsd}/eV	IP_{OVGF}/eV (pole strength)	orbital character	Δ*E*/meV	*m*
p-$C_6H_4Cl_2$	1	9.07	8.67(0.90)	$3b_{3g}(\pi_3)$	-40 ± 60	−0.25
	2	9.92	9.76(0.89)	$1b_{1g}(\pi_2)$	0 ± 60	−0.13
	3	11.33	11.26(0.89)	$3b_{2u}(n_{\|\|})$	(-110 ± 60)	−0.28
	4	11.45	11.35(0.91)	$6b_{3u}(n_\perp)$	(-50 ± 60)	
	5	11.55	11.51(0.91)	$5b_{2g}(n_{\|\|})$	(-70 ± 60)	
	6	12.62	12.85(0.90)	$10a_g$	-30 ± 130	(−0.21)
	7	12.75	12.89(0.90)	$2b_{3g}(n_\perp)$	(-150 ± 100)	−0.29
	8	13.02	13.19(0.90)	$4b_{2g}$	(-0 ± 100)	
	9	13.41	13.78(0.83)	$2b_{2u}(\pi_1)$	-150 ± 110	−0.27
	10	14.55	14.70(0.89)	$9b_{1u}(\sigma_{CCl})$	-40 ± 80	−0.12
	11	14.94	15.08(0.88)	$5b_{3u}$	$+20 \pm 140$	−0.16
	12	15.79	16.11(0.86)	$8b_{1u}$	-30 ± 60	−0.17
	13	16.09	16.18(0.87)	$4b_{3u}$	-50 ± 120	−0.19
	14	17.01	17.30(0.86)	$9a_g$	-20 ± 70	−0.16
	s_1	15.50[a]	–	–	–	−0.16
	s_2	17.43[a]	–	–	–	(−0.12)

[a] Obtained by He*(2^3S) PIES.

least-squares method. Vertical IPs are determined from He I UPS. The peak energy shifts are obtained as the difference between the peak position (E_{PIES}, electron energy scale) and the "nominal" value (E_0 = difference between metastable excitation energy and sample IP): $\Delta E = E_{PIES} - E_0$.

Calculated interaction potential energy curves between the Li(^{2}S) atom and *o*-, *m*-, and *p*-$C_6H_4Cl_2$ by the MP2/6-31+G* level of theory are shown in Figures 10−12. The potential energy curves are shown as a function of (a) the distance *R* between the Li and either Cl atom or the center of the benzene

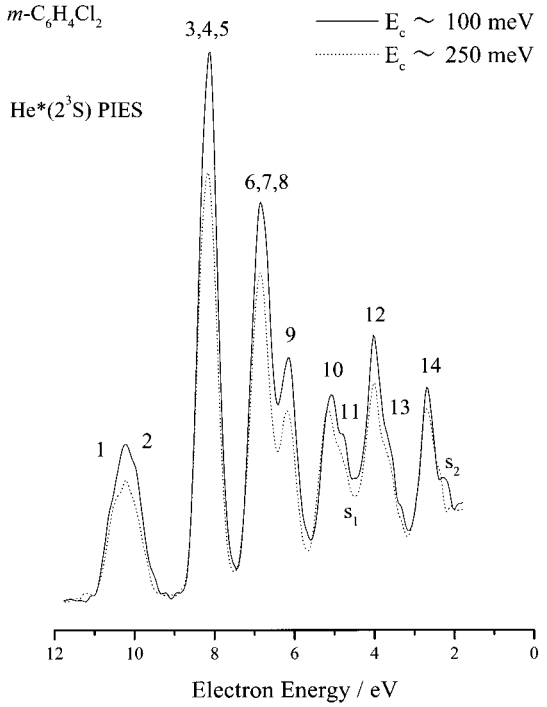

Figure 5. Collision-energy-resolved He*(2³S) PIES of *m*-$C_6H_4Cl_2$. E_c denotes collision energy.

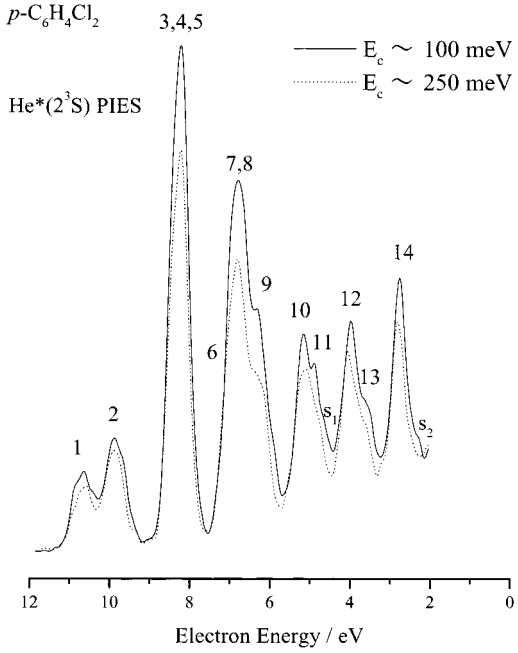

Figure 6. Collision-energy-resolved He*(2³S) PIES of *p*-$C_6H_4Cl_2$. E_c denotes collision energy.

ring, (b) the in-plane angle θ within the molecular plane, and (c) the angle ϕ in the plane parallel to the phenyl ring, in which the distance between the planes is fixed at 2.75 Å.

V. Discussion

UPS and PIES. Photoelectron spectra of dichlorobenzenes have been extensively investigated.[23,46−48] PIES for *o*-, *m*-, and *p*-$C_6H_4Cl_2$ are shown in Figures 1−3 together with UPS. The branching ratios are clearly different compared to those in UPS, which reflect the difference in the ionization mechanism; strong bands in PIES originate from orbitals having large electron density exposed outside the molecular surface. By using this feature of PIES together with calculated IPs via Koopmans' theorem, Fujisawa et al.[49] have proposed band assignments for these compounds. However, the calculated IPs do not reproduce the observed ones well, especially for inner orbitals where the difference becomes more than 3 eV. We have reexamined the assignments on the basis of the characteristics of the 2D-PIES and also of the calculated IPs by the OVGF method. The calculated IPs agree well with the observed whole IPs within 0.4 eV for dichlorobenzenes. Therefore, as summarized in Tables 1−3, more reliable and precise band assignments can be proposed.

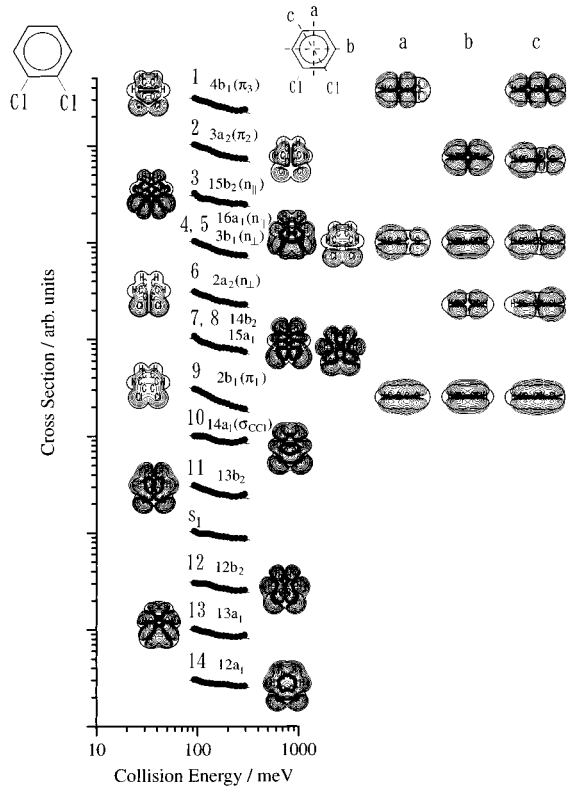

Figure 7. Collision energy dependence of partial ionization cross sections for *o*-$C_6H_4Cl_2$ with He*(2³S) atom. The contour plots show electron density maps for respective MOs. At the right side of the figure, electron density maps for $\pi_{3,2,1}$ and $n_\perp$ orbitals are drawn on the denoted plane, which includes a dashed line and being perpendicular to the molecular plane.

The PIES characteristics of dichlorobenzenes are summarized as follows: (1) The π bands derived mainly from the benzene π orbitals and the *n* bands due to the chlorine 3p orbitals are generally enhanced relative to the other bands (σ type), because the π and *n* orbitals are exposed outside the repulsive molecular surface and hence interact with metastable atoms more efficiently than the σ orbitals, yielding stronger bands in PIES. (2) The $n_{||}$ band due to the Cl 3p orbital distributed parallel with respect to the benzene ring is weak in intensity compared to the $n_\perp$ band distributed perpendicular with respect to the ring, since the $n_{||}$ orbital is shielded by the benzene ring from the attack of a metastable atom. This is clearly observed for *o*-$C_6H_4Cl_2$, while in the case of the other compounds, this shielding effect cannot be examined owing to the overlapping of these bands with neighboring bands. (3) Weak bands S_1 and S_2 appear near $E_c \sim 4.5$ and ~ 2.3 eV in the PIES. The appearance of these bands cannot be interpreted by a simple independent particle model of Penning ionization based on the electron exchange mechanism between the target MO and He 1s orbital. These bands are probably satellite ones arising from the many-body effect.[6,50]

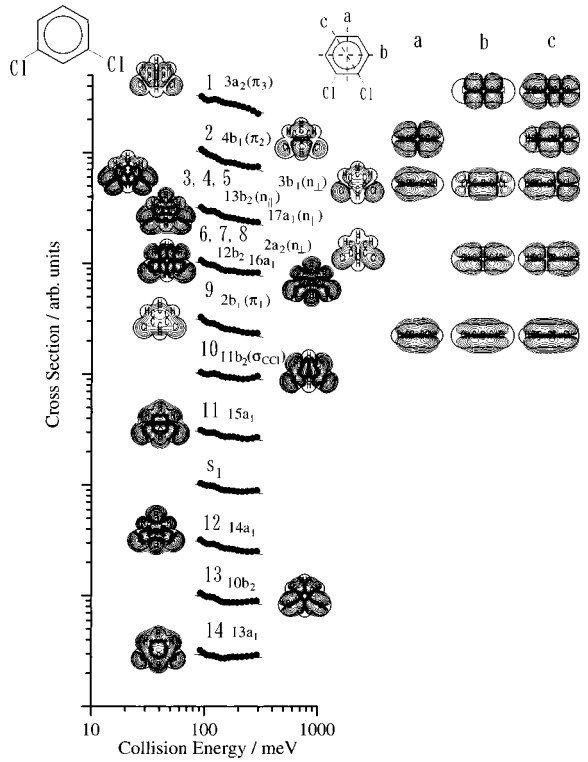

Figure 8. Collision energy dependence of partial ionization cross sections for *m*-$C_6H_4Cl_2$ with He*(2^3S) atom. The contour plots show electron density maps for respective MOs. At the right side of the figure, electron density maps for $\pi_{3,2,1}$ and $n_\perp$ orbitals are drawn on the denoted plane, which includes a dashed line and being perpendicular to the molecular plane.

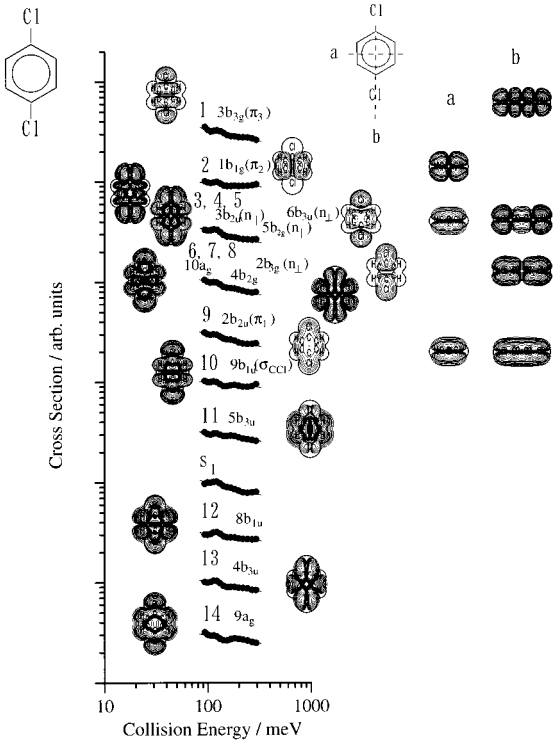

Figure 9. Collision energy dependence of partial ionization cross sections for *p*-$C_6H_4Cl_2$ with He*(2^3S) atom. The contour plots show electron density maps for respective MOs. At the right side of the figure, electron density maps for $\pi_{3,2,1}$ and $n_\perp$ orbitals are drawn on the denoted plane, which includes a dashed line and being perpendicular to the molecular plane.

TABLE 4: Relative PIES Intensities of $n_{||}$, σ_{CF}, and π_F Bands in *o*-, *m*-, and *p*-$C_6H_4Cl_2$

compounds	I(n)/ $I(\pi_3, p_2)$	$I(\pi_1)$/ $I(\pi_3, \pi_2)$	I(band14)/ $I(\pi_3, \pi_2)$	$m(\pi_1)$/ $I(\pi_3, \pi_2)$
o-$C_6H_4Cl_2$	1.29 ± 0.05	1.33 ± 0.07	1.09 ± 0.07	1.5 ± 0.1
m-$C_6H_4Cl_2$	1.36 ± 0.05	1.26 ± 0.08	0.80 ± 0.15	1.0 ± 0.1
p-$C_6H_4Cl_2$	1.33 ± 0.05	1.28 ± 0.09	1.03 ± 0.10	1.4 ± 0.1

Relative Reactivity of Orbitals with the He*(2^3S) Atom. As mentioned in the introductory section, the Penning ionization reaction can be related to the electrophilic reaction. Moreover, the relative band intensity of PIES is closely related to the reactivity of the corresponding target MO. Therefore, we will discuss the relative reactivity of orbital with the He* atoms on the basis of relative PIES intensity of several specific bands. The PIES intensity of each band was obtained by integrating the corresponding band area. In the case of overlapping bands, a proper deconvolution was made.

(i) Reactivity of the $\pi_{3,2,1}$ Orbitals. As can be seen in Figures 1−3 and also as summarized in Table 4, the intensities of the π_1 bands for dichlorobenzenes are larger than those of the $\pi_{3,2}$ bands. In the table, $I(\pi_1)$ is the integrated intensity of the π_1 band, and $I(\pi_3, \pi_2)$ is the average intensity of the $\pi_{3,2}$ bands. It is noted that the magnitude of $I(\pi_1)$ is 1.2−1.3 times larger than that of $I(\pi_3,\pi_2)$. This is because electron densities of the π_1 orbitals resulted from the conjugation between the C 3p orbitals and Cl orbitals for the investigated compounds are larger than those of $\pi_{3,2}$ orbitals. Moreover, the ratio of the relative PIES intensity of π_1 orbital $I(\pi_1)$ to the average intensity of π_3 and π_2 orbitals $I(\pi_3,\pi_2)$ for *o*-$C_6H_4Cl_2$ is clearly larger than that corresponding to the *m* and *p*-$C_6H_4Cl_2$ as summarized in Table 4. This is closely correlated to the larger electron density of π_1 orbital for *o*-$C_6H_4Cl_2$ around the Cl atoms than that of either *m*- or *p*-$C_6H_4Cl_2$. It is also noted that the perpendicular approach of the He* atom to the phenyl ring toward the Cl atoms shown in Figures 10c, 11c, and 12c indicates the larger attractive interaction for *o*-$C_6H_4Cl_2$ compared to that of the other compounds. This attractive force, furthermore, discriminates the orbital reactivity among the compounds.

Elucidation of orbital reactivity for π_3 and π_2 orbital for the *o*- and *m*-$C_6H_4Cl_2$ is not straightforward since the π_3 and π_2 bands in the PIES overlapped each other. However, the appropriate deconvolution of the π_3 and π_2 bands provided slightly larger PIES intensity for the π_2 band than that of the π_3 band. For *p*-$C_6H_4Cl_2$, the PIES intensity of the π_2 band is about 1.5 times stronger than that of the π_3 band. Similar orbital reactivity between the π_3 and π_2 orbitals has been reported for *p*-$C_6H_4F_2$,[13] while the π_2/π_3 PIES intensity ratio (∼2) for *p*-$C_6H_4F_2$ is slightly larger than that (∼1.5) for *p*-$C_6H_4Cl_2$. This is due to the fact that there is a certain electron density around the Cl atoms in π_3 orbital for *p*-$C_6H_4Cl_2$ as shown in Figure 9, while for *p*-$C_6H_4F_2$ there is no apparent electron density around the F atoms of the π_3 orbital. It should be noted that the π_2 orbital in both compounds is almost equivalent to the π_2 orbital of benzene. This result also implies that the orbital reactivity around the Cl atom lone pair region perpendicular to the phenyl ring is slightly smaller than that of the π orbital reactivity, taking into account the nodal plane effect of the phenyl ring. In other words, as was found in the case of difluorobenzenes,[13] the larger electron density region of the phenyl ring brings the larger reactivity toward the He* atom, and it plays a more dominant role compared to the electron distribution localized at the Cl atoms for these orbitals. Therefore, the larger reactivity of the π_2 orbital compared to the π_3 orbital for *o*- and *m*-$C_6H_4Cl_2$ can also be well-interpreted from the electron density distributions

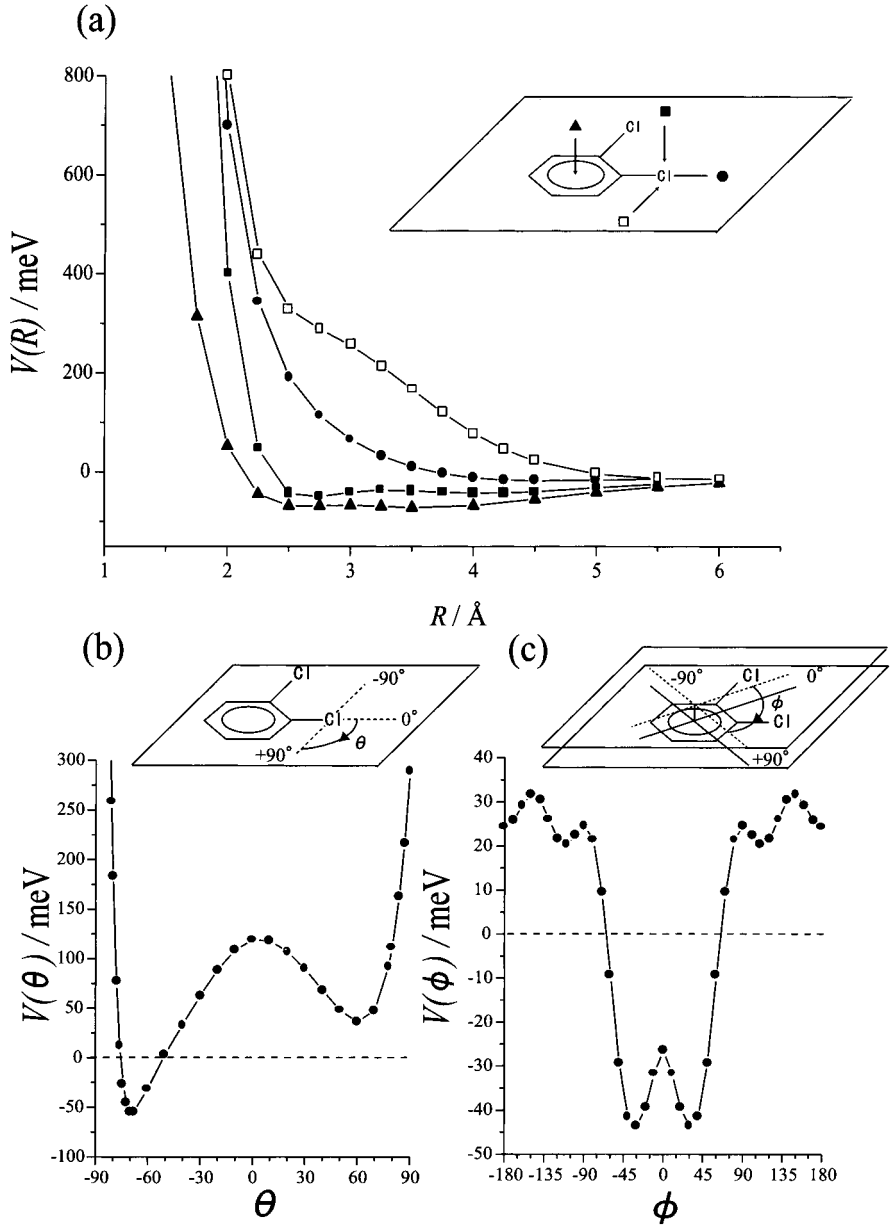

Figure 10. Interaction potential curves V(R) obtained by MP2 calculations for *o*-$C_6H_4Cl_2$ and Li as a function of distance R, out-of-plane access to the center of the benzene ring (▲), in-plane collinear access to the C−Cl bond (●), out-of-plane perpendicular access to the C−Cl bond (■), in-plane perpendicular access to the C−Cl bond (□). Note that R is defined from the center of the benzene ring for (▲) direction, while for the others, (●), (■), and (□), R is defined from the Cl atom. (b) Interaction potential curve $V(\theta)$ as a function of the in-plane angle θ centered at the Cl atom. Distance between the Li and Cl atoms is fixed at 2.75 Å. (c) Interaction potential curve $V(\phi)$ as a function of the angle ϕ. The distance between the center of rotation defined in the figure and Li atom is fixed at 3.127 Å. Note that the distance between the molecular plane and rotation plane is 2.75 Å.

of these orbitals, since the electron distribution of phenyl ring region of the π_2 orbital extends over a larger area than that of π_1 orbital.

The general order of the π orbital reactivity can be summarized as follows:

$$\pi_1 > \pi_2 > \pi_3$$

(ii) Relative Reactivity of Other Orbitals with Respect to π Orbitals. In Table 4, we summarized the orbital reactivity of the n and σ_{CH} (band 14) orbitals. Here, $I(n)$ is the average intensity of the three n bands (two $n_{||}$ bands and one $n_{\perp}$ band) having higher electron energy, $I(n) = [2I(n_{||}) + I(n_{\perp})]$, and $I(\pi_3,\pi_2)$ is that of π_3 and π_2. As can be recognized from the table, the $I(n)/I(\pi_3,\pi_2)$ value for *o*-$C_6H_4Cl_2$ is slightly smaller than the $I(n)/I(\pi_3,\pi_2)$ values of *m*- and *p*-$C_6H_4Cl_2$. An identical tendency has been already reported, while their absolute values are different, which may be reflective of the different collision energies of the He* atoms between the present and previous studies. From these values, Fujisawa et al.[49] suggested that the smaller value of the *o*-$C_6H_4Cl_2$ was attributed to the shielding effect of the $n_{||}$ orbital from the attack of the He* by the Cl atom as well as by the phenyl ring owing to the close proximity of the two Cl atoms. Although it should be true, it is very hard to estimate an exact contribution of the $n_{||}$ component to $I(n)$ because of the serious overlapping with the other n orbitals. As mentioned in the last section, a wider electron distribution around the phenyl ring region brings a larger reactivity with respect to that of the Cl atom lone pair regions. Therefore, it is natural that major contribution for the strongest peak assigned

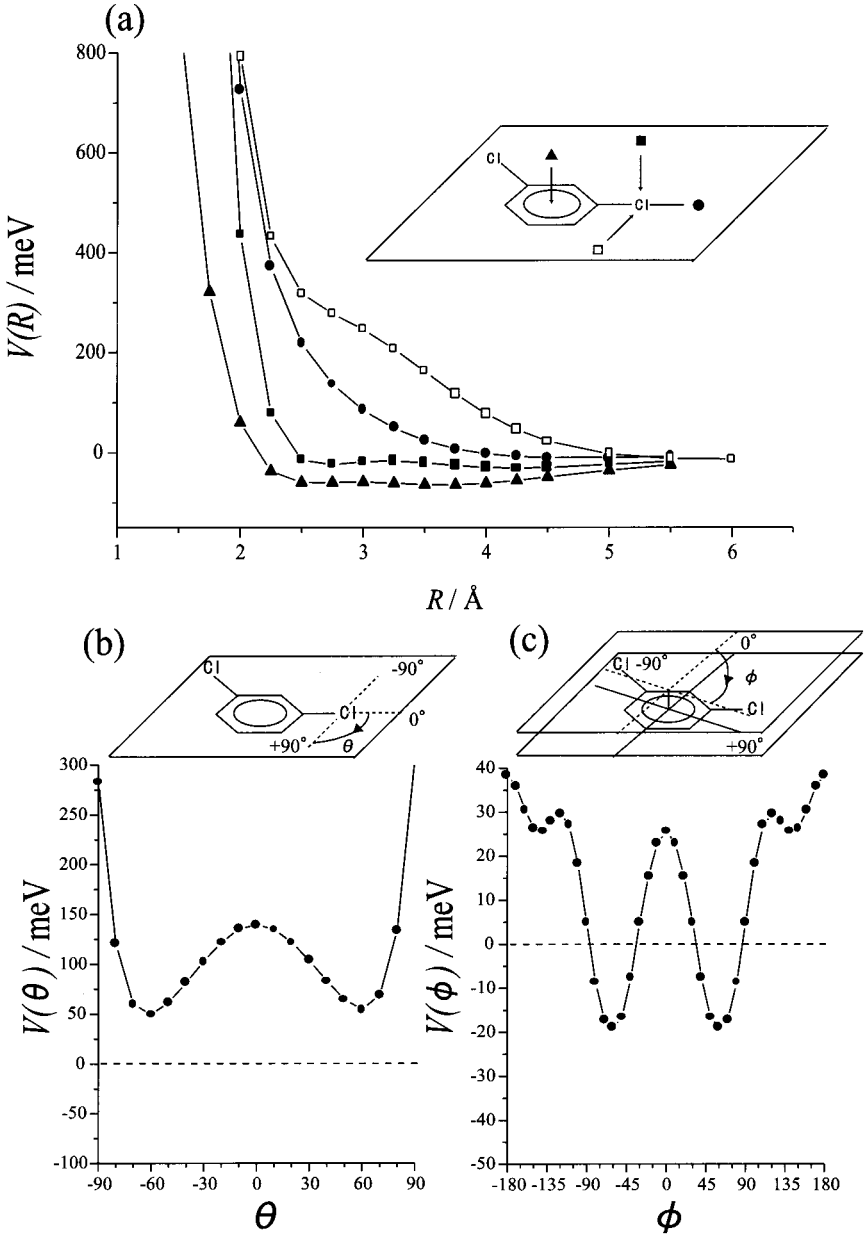

Figure 11. Interaction potential curves V(R) obtained by MP2 calculations for m-$C_6H_4Cl_2$ and Li as a function of distance R, out-of-plane access to the center of the benzene ring (▲), in-plane collinear access to the C−Cl bond (●), out-of-plane perpendicular access to the C−Cl bond (■), in-plane perpendicular access to the C−Cl bond (□). Note that R is defined from the center of the benzene ring for (▲) direction, while for the others, (●), (■), (□), R is defined from the F atom. (b) Interaction potential curve $V(\theta)$ as a function of the in-plane angle θ centered at the Cl atom. Distance between the Li and Cl atoms is fixed at 2.75 Å. (c) Interaction potential curve $V(\phi)$ as a function of the angle ϕ . The distance between the center of rotation defined in the figure and Li atom is fixed a 3.113 Å. Note that the distance between the molecular plane and rotation plane is 2.75 Å.

to bands 4 and 5 and bands 3−5 can be ascribed to the $n_{||}$ orbital among the dichlorobenzenes. As a consequence, a definite explanation for propensity of the orbital reactivity among the compounds cannot be attained.

Next, we will discuss the differences in the relative intensity of band 14(σ_{CH}) in PIES among the dichlorobenzenes. It is obvious that the relative PIES intensity of band 14 for the o-$C_6H_4Cl_2$ is larger than the relative PIES intensities of band 14 of m-and p-$C_6H_4Cl_2$. Fujisawa et al.[49] have also found the similar propensity, and they attributed this difference to the shielding effect of the Cl atoms among the compounds. They interpreted as the shielding effect for the o-$C_6H_4Cl_2$ would be smaller as compared to the shielding effects of the other compounds because the adjacent two Cl atoms of o-$C_6H_4Cl_2$ more or less could counteract their shielding effect on each other. However, electron density maps for the corresponding MOs shown in Figures 7−9 imply that the electron densities around the Cl atoms for these orbitals do not play an important role on the ionization because of their poor penetration from the molecular surface. On the other hand, the electron density distribution around the C−H bonds extends further from the molecular surface, and it should be responsible for the different orbital reactivity among the compounds. The difference can be raised from the variation of electron distribution owing to nodal planes around the Cl atoms. For the o-$C_6H_4Cl_2$, there is a nodal plane between Cl atoms and the phenyl ring, while for o-and m-$C_6H_4Cl_2$, there are two nodal planes. As a result, electron distribution around the C−H bonds for o-$C_6H_4Cl_2$ extends over the larger region than the ones for the m- and p-$C_6H_4Cl_2$. It is noted that the electron distributions of MOs around the C−H

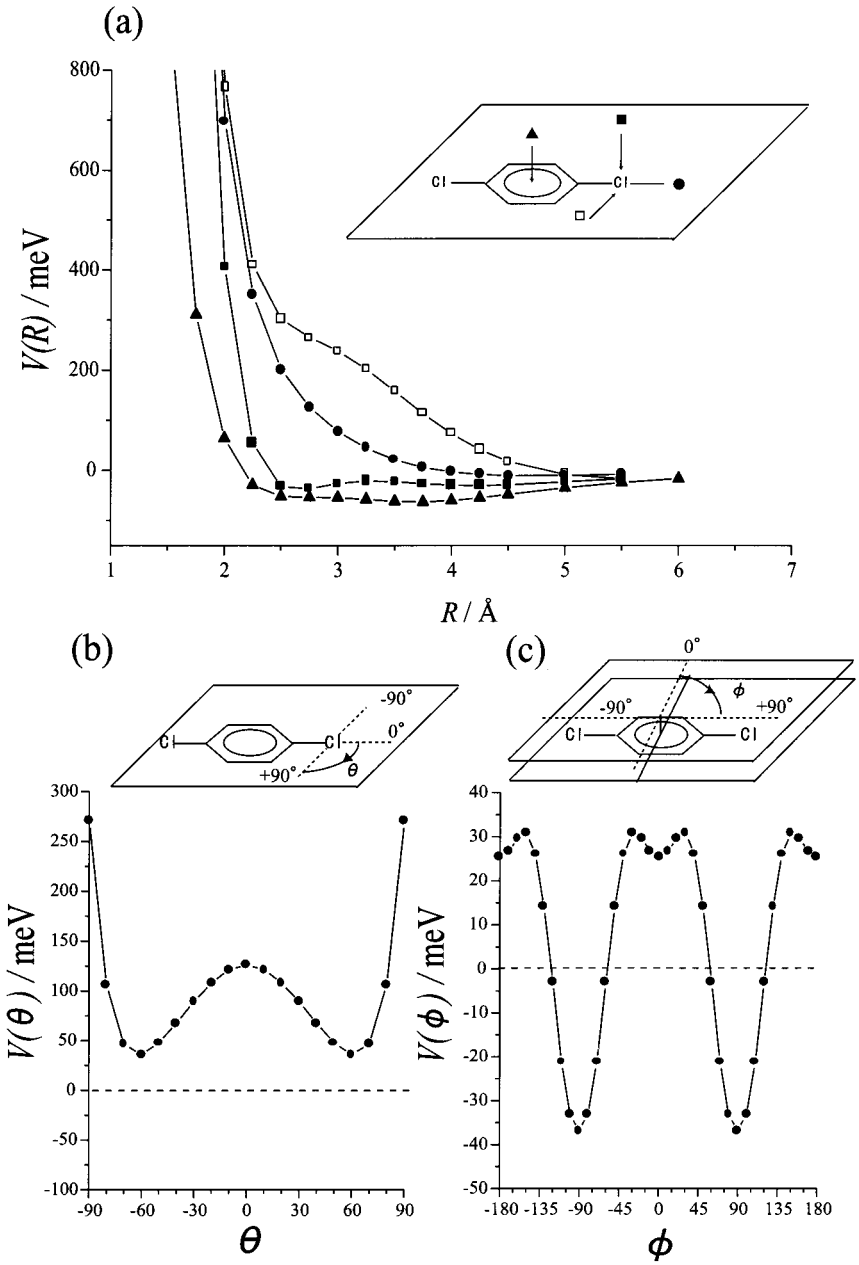

Figure 12. Interaction potential curves V(R) obtained by MP2 calculations for p-$C_6H_4Cl_2$ and Li as a function of distance R, out-of-plane access to the center of the benzene ring (▲), in-plane collinear access to the C−Cl bond (●), out-of-plane perpendicular access to the C−Cl bond (■), in-plane perpendicular access to the C−Cl bond (□). Note that R is defined from the center of the benzene ring for (▲) direction, while for the others, (●), (■), (□), R is defined from the Cl atom. (b) Interaction potential curve $V(\theta)$ as a function of the in-plane angle θ centered at the Cl atom. Distance between the Li and Cl atoms is fixed at 2.75 Å. (c) Interaction potential curve $V(\phi)$ as a function of the angle ϕ . The distance between the center of rotation defined in the figure and Li atom is fixed at 3.123 Å. Note that the distance between the molecular plane and rotation plane is 2.75 Å.

bonds corresponding to bands 14 for the *o*-and *m*-compounds are separated by the two nodal planes. Moreover, the larger PIES intensity for the *p*-compound than for the *m*-compound can be ascribed to the larger electron density around the Cl atoms. Thus, the ordering of the relative intensity of the bands *o*- > *p*- > *m*-$C_6H_4Cl_2$ can be explained in terms of the different electron distribution around the C−H bonds and Cl atoms among the compounds.

Collision Energy Dependence of the Partial Ionization Cross Sections (CEDPICS). *(i) o-$C_6H_4Cl_2$.* Strong negative slopes for the CEDPICS (Figure 7) of the π bands (bands 1, 2, and 9) and the $n_{||}$ and $n_{\perp}$ bands (bands 3−6) indicate attractive interactions for the out-of-plane direction of phenyl ring and the $n_{\perp}$ orbital region. When an attractive interaction plays a dominant role, the collision energy dependence of the ionization cross section shows a negative slope because slower He* metastable atoms can approach the reactive region effectively and then ionization cross section is enhanced for lower collision energies. As shown in Figure 10a, a theoretical calculation indicated attractive interactions for the out-of-plane of the phenyl ring and the $n_{\perp}$ orbital region with a well depth of about 70 and 50 meV, respectively, while it does not show an attractive interaction for perpendicular direction to C−Cl axis (□) because of the neighboring H atoms for this direction in accord with the case of monochlorobenzene.[12] However, Figure 10b shows an evidence of attractive interaction around the Cl atoms correlated to the $n_{||}$ orbital region. A deeper attractive well was found for the midway point between the two Cl atoms. In fact,

negative peak energy shifts were observed for these bands, which again indicate the existence of an attractive well whose depth is ranging from 40 to 100 meV. Although it seems that the well depth is too small to give a strong negative slope of the CEDPICS for π and *n* bands, very recently we have reported that an attractive effect around the reaction point becomes stronger with increasing the width (spatial extension) of a potential well.[13] Indeed, calculated potentials for the out-of-plane direction of the phenyl ring and the $n_\perp$ orbital region have a wider potential well. The very strong negative slope for the CEDPICS (Figure 7) of the π_1 bands compared to the other compounds can be ascribed to a wider electron distribution, which indicates an attractive interaction, in the direction perpendicular to the phenyl ring around the Cl atoms. It also indicates that the mutual through-space interaction of the out-of-plane lone pairs is much stronger than their interaction with the ring π orbitals. A similar effect was observed for the $n_{||}$ band of *o*-$C_6H_4F_2$.[13]

It is noteworthy that relatively strong negative slopes for the CEDPICS of the remaining bands were observed. It may be puzzling here because there are larger electron distributions around the collinear direction with respect to the C−Cl axis and around the C−H bonds, which generally show repulsive interactions. Calculated interaction potential shows a repulsive character along C−Cl axis direction and around the C−H bonds, while at long range (5−7 Å) a small attractive (∼10 meV) character around the C−H bonds was found. However, the well depth of this order does not show a dominant role, since it is sufficiently small compared to the collision energy. In fact, in the case of monochlorobenzene,[12] slope parameters of the corresponding bands ranging from −0.09 to −0.01 imply that the ionization are not dominated by the attractive interaction. Although a direct comparison of the absolute values between the different measurements of monochlorobenzene and dichlorobenzenes cases is difficult owing to each experimental error, the difference among these compounds is trustworthy. As indicated by the previous paper,[13] a wider attractive potential can affect some of He* atoms trajectories and convey the He* atoms toward the exterior region of MOs, where the repulsive interaction is dominant. It is noted that the Cl atom substitution from monochlorobenzene to dichlorobenzenes can generate the another wider attractive region around the Cl atom. Therefore, it is reasonable to observe the larger attractive effect for dichlorobenzenes than that for monochlorobenzene.

(ii) m-$C_6H_4Cl_2$. A strong negative slope was observed in CEDPICS for bands 1−9 mainly corresponding to the π and $n_{||}$ and $n_\perp$ orbitals, which indicates attractive interaction around the π orbital of the phenyl ring and $n_\perp$ orbital region in accord with the calculated interaction potential curves shown in Figure 11. Although some of them were seriously overlapped with neighboring bands and actually it is hard to estimate each contribution, similarities of absolute values of CEDPICS for the $\pi_{3,2}$ and n bands to those for the corresponding bands in *o*-$C_6H_4Cl_2$ can be recognized within experimental error. Theoretical calculations also indicate well resemblance of interaction potentials for Li-*o*-$C_6H_4Cl_2$ and Li-*m*-$C_6H_4Cl_2$ systems except for the $n_{||}$ orbital region. Experimental results indicate that either $n_{||}$ orbital region shows a attractive nature as previously concluded in the case of monochlorobenzene[12] or a major contribution of the overlapped bands 3− 5 is ionization from the $3b_1(n_\perp)$ orbital.

The remaining bands (bands 10−14) also show negative CEDPICS similar to the case of *o*-$C_6H_4Cl_2$. As was mentioned above, this is because the wider potential well around the π orbital region of the phenyl ring and Cl atom lone pair regions are important for ionization event. Thus, a negative slope of CEDPICS for these bands was observed. Change in the degrees of the slope parameters for these bands could be interpreted by taking an anisotropic electron density distribution around the molecule for each MO into account. It is also noted that attractive interaction of the Cl atom lone pair regions was predicted to be small compared to the *o*-$C_6H_4Cl_2$ as can be seen in Figures 10 and 11. Thus, the attractive effects around the out-of-plane direction of the phenyl ring and Cl atom lone pair regions for ionization becomes less dominant than those for *o*-$C_6H_4Cl_2$, and they give slightly smaller absolute values of the slope for these bands. This is clearly observed in the CEDPICS (−0.05) for band 14.

(iii) p-$C_6H_4Cl_2$. A strong negative slope was observed in CEDPICS for the π bands and n bands as in the cases of *o*- and *m*-$C_6H_4Cl_2$.

It is noted that absolute slope value of CEDPICS for each band for *p*-$C_6H_4Cl_2$ are almost equivalent to that of the corresponding band for *o*-$C_6H_4Cl_2$ except for the π_1 and π_2 bands. This finding suggests that the reactively and interaction of each MO upon the electrophilic attack of the He* atoms is almost equivalent between *o*- and *p*-$C_6H_4Cl_2$. This is also supported by the theoretical calculation as recognized their similarity between the calculated interaction potentials of *o*- and *p*-$C_6H_4Cl_2$ with Li atom as shown in Figures 10 and 12 except for the $n_{||}$ orbital region. Relatively small absolute value of CEDPICS for band 2 compared to the other *o*- and *m*-$C_6H_4Cl_2$ can be ascribed to the fact that the π_2 orbital for *p*-$C_6H_4Cl_2$ has no Cl 3p perpendicular component with respect to the phenyl ring. The electron density distribution of the π_2 orbital for *p*-$C_6H_4Cl_2$ is almost equivalent to that for benzene. It is important to realize that the out-of-plane direction of the phenyl ring on Cl atoms shows an attractive interaction for dichlorobenzenes. Therefore, the slope of CEDPICS of π_2 (band 2) for *p*-$C_6H_4Cl_2$ becomes smaller than that for the other compounds.

The collision-energy-resolved PIES (CERPIES) results for these compounds as shown in Figure 6 indicate a very interesting feature of the π_3 band. Namely, it looks as if the peak position of this band moves toward lower electron energy with increasing collision energy, although the peak position of a band should move toward higher electron energy with increasing collision energy such as band 14. Thus, this observation implies that the π_3 band may contain at least two components. The π_3 orbital of this compound has a larger electron density around the Cl atoms and phenyl ring region. Therefore, it is natural that the π_3 band contains two components. As a consequence, a curious feature of CERPIES of this band was observed since the two components overlapped each other in the band and the extent of their overlapping varied as collision energy dependence of the each component. Similar observations are also expected for the π_3 and π_2 bands in the CERPICS of *o*- and *m*-$C_6H_4Cl_2$. However, these bands are partially overlapped with each other in the spectra; as a result, it was not clearly observed as can be seen in Figures 4 and 5.

(iv) Attractive Interactions around the π_1 and $n_\perp$ Orbital Regions. Recently, we have reported that the magnitude of the attractive interaction around the $n_{||}$ and σ_{CF} orbital region was larger for *o*-$C_6H_4F_2$ than that for *m*- and *p*-$C_6H_4F_2$ among the difluorobenzenes.[13] The present results do not show a strong preference for the attractive interaction around the $n_{||}$ and σ_{CCl} orbital region among the dichlorobenzenes. This difference can be ascribed to the distinct anisotropic interaction around halogen

atom effect between the F-atom-containing compounds and the Cl-atom-containing ones. Namely, the attractive interaction is localized in-plane around the collinear direction with respect to the C−F axis for F-atom-containing compounds, while the attractive interaction is found around the perpendicular directions with respect to the C−Cl axis for Cl-atom-containing compounds. Therefore, in the case of *o*-$C_6H_4F_2$, the two closely proximate F atoms can generate a wider attractive region for the $n_{||}$ and σ_{CF} orbital regions than that for the others, *m*- and *p*-$C_6H_4F_2$. As a consequence, a larger attractive effect was observed in these orbital regions for *o*-$C_6H_4F_2$, since the attractive effect around the reaction point becomes stronger with increasing width of the attractive region. This is not the case for *o*-$C_6H_4Cl_2$, reflecting the difference of the anisotropic interaction around the halogen atoms between *o*-$C_6H_4Cl_2$ and *o*-$C_6H_4F_2$. However, a similar effect was observed for π_1 band for *o*-$C_6H_4Cl_2$ since two closely proximate Cl atoms *produced* a wider attractive well for the perpendicular direction respective to the phenyl ring as can be seen in Figure 10c.

Interaction potential curves in Figures 10c−12c clearly indicated that the order of the attractive interaction around the lone pair region of Cl atoms perpendicular to the phenyl ring became *o*- > *p*- > *m*-$C_6H_4Cl_2$. To compare the relative magnitude of the attractive interaction for the $n_\perp$ orbital region experimentally among the dichlorobenzenes, a comparison of the slope parameters for the $n_\perp$ bands is the most appropriate. However, some of the bands seriously overlapped with the neighboring bands, and then, unfortunately, a direct comparison among the compounds is unattainable. It is very helpful to use the π_1 bands instead of the $n_\perp$ bands, because the electron density of the π_1 orbitals and also their magnitude of attractive interaction for the phenyl ring region are almost equivalent. Therefore, a major difference of the attractive interaction for the π_1 bands can be ascribed to the distinct attractive interaction around the Cl atom lone pair region perpendicular to the phenyl ring, and then, the ratio $m(\pi_1)/m(\pi_{3,2})$ was evaluated, where $m(\pi_{3,2})$ was the average slope parameter of the π_3 and π_2 bands as summarized in Table 4. The interaction for the *p*-compound may be overestimated by this procedure because only π_2 orbital for the *p*-compound has no Cl atom 3p character. Therefore, it is reasonable to conclude the magnitude of the attractive interaction around the $n_\perp$ orbital region to be *o*- > *p*- > *m*-$C_6H_4Cl_2$.

VI. Conclusion

In this study, the results of PIES of *o*-, *m*-, and *p*-$C_6H_4Cl_2$ with metastable He*(2^3S) atom were presented. Highly anisotropic interactions around the Cl atoms are obtained. It is found that CEDPICS results of the $\pi_{3,2,1}$ and $n_\perp$ bands show the attractive interactions for these compounds. Observed CEDPCIS of the remaining bands among these compounds was almost identical, and it indicates a slightly larger attractive effect than the case of the monochlorobenzene. The latter finding implies that the Cl atom substitution of monochlorobenzene into dichlorobenzenes yields larger attractive effect for the Penning ionization process.

Furthermore, we discussed the relative reactivity of $\pi_{3,2,1}$, n, and σ_{CH} orbitals. The present results indicate that the reactivity of the orbitals are closely related to the anisotropic interaction around the molecule.

Acknowledgment. This work has been partially supported by a Grant in Aid for Scientific Research from the Japanese Ministry of Education, Science, and Culture. One of the authors (K.I.) thanks the Japan Society for the Promotion of Science (JSPS) for a JSPS Research Fellowship.

References and Notes

(1) Penning, F. M. *Naturwissenschaften* **1927**, *15*, 818.
(2) Hotop, H.; Niehaus, A. *Z. Phys*. **1969**, *228*, 68.
(3) Ohno, K.; Mutoh, H.; Harada, Y. *J. Am. Chem. Soc*. **1983**, *105*, 4555.
(4) Ohno, K.; Matsumoto, S.; Harada, Y. *J. Chem. Phys*. **1984**, *81*, 4447.
(5) Ohno, K.; Yamakado, H.; Ogawa, T.; Yamata, T. *J. Chem. Phys*. **1996**, *105*, 7536.
(6) Takami, T.; Ohno, K. *J. Chem. Phys.* **1992**, *96*, 6523.
(7) Yamauchi, M.; Yamakita, Y.; Yamakado, H.; Ohno, K. *J. Electron Spectrosc. Relat. Phenom*. **1998**, *88*−*91*, 155.
(8) Kishimoto, N.; Yamakado, H.; Ohno, K. *J. Phys. Chem. A* **1996**, *100*, 8204.
(9) Yamakita, Y.; Yamauchi, M.; Ohno, K. *Chem. Phys. Lett*. **2000**, *322*, 189.
(10) Kishimoto, N.; Ohno, K. *J. Phys. Chem. A* **2000**, *104*, 6940.
(11) Kishimoto, N.; Furuhashi, M.; Ohno, K. *J. Electron Spectrosc. Relat. Phenom*. **2000**, *113*, 35.
(12) Imura, K.; Kishimoto, N.; Ohno, K. *J. Phys. Chem*. *A* **2001**,*105*, 4189.
(13) Imura, K.; Kishimoto, N.; Ohno, K. *J. Phys. Chem*. *A* **2001**, *105*, 6073.
(14) Imura, K.; Kishimoto, N.; Ohno, K. *J. Phys. Chem*. *A* **2001**, *105*, 6378.
(15) Tokue, I.; Sakai, Y.; Yamasaki, K. *J. Chem. Phys.* **1997**, *106*, 4491.
(16) Alberti, M.; Lucas, J. M.; Brunetti, B.; Pirani, F.; Stramaccia, M.; Rosi, M.; Vecchiocattivi, F. *J. Phys. Chem*. *A* **2000**, *104*, 1405.
(17) Yamato, M.; Okada, S.; Wu, V. W.-K.; Ohoyama, H.; Kasai, T. *J. Chem. Phys*. **2000**, *113*, 6673.
(18) Yamato, M.; Ohoyama, H.; Kasai, T. *J. Phys. Chem. A* **2001**, *105*, 2967.
(19) Mitsuke, K.; Takami, T.; Ohno, K. *J. Chem. Phys*. **1989**, *91*, 1618.
(20) Ohno, K.; Takami, T.; Mitsuke, K.; Ishida, T. *J. Chem. Phys*. **1991**, *94*, 2675.
(21) Takami, T.; Mitsuke, K. Ohno, K. *J. Chem. Phys*. **1991**, *95*, 918.
(22) Gardner, J. L.; Samson, J. A. R. *J. Electron Spectrosc. Relat. Phenom*. **1976**, *8*, 469.
(23) Kimura, K.; Katsumata, S.; Achiba, Y.; Yamazaki, T.; Iwata, S. *Handbook of He I Photoelectron Spectra of Fundermental Organic Molecules*; Japan Scientific: Tokyo, 1981.
(24) Turner, D. W.; Baker, C.; Baker, A. D.; Brundle, C. R. *Molecular Photoelectron Spectroscopy*; Wiley: London, 1970.
(25) Yee, D. S. C.; Stewart, W. B.; Mcdowell, C. A.; Brion, C. E. *J. Electron Spectrosc. Relat. Phenom*. **1975**, *7*, 93.
(26) Hotop, H.; Hubler, G. *J. Electron Spectrosc. Relat. Phenom*. **1977**, *11*, 101.
(27) (a) Auerbach, D. J. *Atomic and Molecular Beam Methods*; Scoles, G., Ed.; Oxford University: New York, 1988; p 369. (b) Kishimoto, N.; Aizawa, J.; Yamakado, H.; Ohno, K. *J. Phys. Chem. A* **1997**, *101*, 5038.
(28) Rothe, E. W.; Neynaber, R. H.; Trujillo, S. M. *J. Chem. Phys*. **1965**, *42*, 3310.
(29) Illenberger, E.; Niehaus, A. *Z. Phys. B* **1975**, *20*, 33.
(30) Parr, T.; Parr, D. M.; Martin, R. M. *J. Chem. Phys*. **1982**, *76*, 316.
(31) Hotop, H. *Radiat. Res*. **1974**, *59*, 379.
(32) Haberland, H.; Lee, Y. T.; Siska, P. E. *Adv. Chem. Phys*. **1981**, *45*, 487.
(33) Hotop, H.; Roth, T. E.; Ruf, M.-W.; Yencha, A. J. *Theor. Chem. Acc*. **1998**, *100*, 36.
(34) Yamakado, H.; Yamaguchi, M.; Hoshino, S.; Ohno, K. *J. Phys. Chem*. **1995**, *99*, 55.
(35) Ohno, K.; Yamakado, H.; Ogawa, T.; Yamata, T. *J. Chem. Phys*. **1996**, *105*, 7536.
(36) Ohno, K.; Kishimoto, N.; Yamakado, H. *J. Phys. Chem.* **1995**, *99*, 9687.
(37) Yamakado, H.; Okamura, K.; Ohshimo, K.; Kishimoto, N.; Ohno, K. *Chem. Lett*. **1997**, 269.
(38) Kishimoto, N.; Ohshimo, K.; Ohno, K. *J. Electron Spectrosc. Relat. Phenom*. **1999**, *104*, 145.
(39) Kishimoto, N.; Osada, Y.; Ohno, K. *J. Phys. Chem*. *A* **2000**, *104*, 1393.
(40) Doraiswamy, S.; Sharma, S. *J. Mol. Struct.* **1983**, *102*, 81.
(41) Domenicano, A.; Schultz, G.; Hargittai, I. *J. Mol. Struct.* **1982**, *78*, 97.
(42) Pauling, L. *The Nature of the Chemical Bond*; Cornell University: Ithaca, New York, 1960.
(43) von Niessen, W.; Schirmer, J.; Cederbaum, L. S. *Comput. Phys. Rep.* **1984**, *1*, 57.

(44) (a) Zakrzewski, V. G.; Ortiz, J. V. *Int. J. Quantum Chem. Symp.* **1994**, *28*, 23. (b) Zakrzewski, V. G.; Ortiz, J. V. *Int. J. Quantum Chem.* **1995**, *53*, 583.

(45) Frisch, M. J.; Trucks, G. W.; Schlegel, H. B.; Scuseria, G. E.; Robb, M. A.; Cheeseman, J. R.; Zakrzewski, V. G.; Montgomery, J. A., Jr.; Stratmann, R. E.; Burant, J. C.; Dapprich, S.; Millam, J. M.; Daniels, A. D.; Kudin, K. N.; Strain, M. C.; Farkas, O.; Tomasi, J.; Barone, V.; Cossi, M.; Cammi, R.; Mennucci, B.; Pomelli, C.; Adamo, C.; Clifford, S.; Ochterski, J.; Petersson, G. A.; Ayala, P. Y.; Cui, Q.; Morokuma, K.; Malick, D. K.; Rabuck, A. D.; Raghavachari, K.; Foresman, J. B.; Cioslowski, J.; Ortiz, J. V.; Baboul, A. G.; Stefanov, B. B.; Liu, G.; Liashenko, A.; Piskorz, P.; Komaromi, I.; Gomperts, R.; Martin, R. L.; Fox, D. J.; Keith, T.; Al-Laham, M. A.; Peng, C. Y.; Nanayakkara, A.; Challacombe, M.; Gill, P. M. W.; Johnson, B.; Chen, W.; Wong, M. W.; Andres, J. L.; Gonzalez, C.; Head-Gordon, M.; Replogle, E. S.; Pople, J. A. *Gaussian 98*; Gaussian, Inc.: Pittsburgh, PA, 1998.

(46) Streets, D. G.; Ceaser, G. P. *Mol. Phys*. **1973**, *26*, 1037.

(47) Ruščić, B.; Klasinc, L.; Wolf, A.; Knop, J. V. *J. Chem. Phys*. **1981**, *85*, 1486.

(48) Potts, A. W.; Lyus, M. L.; Lee, E. P. F.; Fattahallah, G. H. *J. Chem. Soc., Faraday Trans. 2* **1980**, *76*, 556.

(49) Fujisawa, S.; Oonishi, I.; Masuda, S.; Ohno, K.; Harada, Y. *J. Phys. Chem*. **1991**, *95*, 4250.

(50) Masuda, S.; Aoyama, M.; Ohno, K.; Harada, Y. *Phys. Rev. Lett*. **1990**, *65*, 3257.